Accepted Manuscript

Detecting NQR signals severely polluted by interference

Weihang Shao, Jamie Barras, Kaspar Althoefer, Panagiotis Kosmas

PII: S0165-1684(17)30128-7
DOI: 10.1016/j.sigpro.2017.03.032
Reference: SIGPRO 6444

To appear in: *Signal Processing*

Received date: 27 September 2016
Revised date: 13 February 2017
Accepted date: 28 March 2017

Please cite this article as: Weihang Shao, Jamie Barras, Kaspar Althoefer, Panagiotis Kosmas, Detecting NQR signals severely polluted by interference, *Signal Processing* (2017), doi: 10.1016/j.sigpro.2017.03.032

HIGHLIGHTS

- The proposed method effectively cancels complicated interference which can be strong, nonstationary, and have frequencies close to that of signal of interest.
- The proposed method facilitates a valid detection of the NQR signal severely polluted by interference.
- The proposed method performs better than general frequency selective methods of interference cancellation.

Detecting NQR signals severely polluted by interference

Weihang Shao,[1] Jamie Barras,[1] Kaspar Althoefer,[1,2] and Panagiotis Kosmas[1]

[1]*Department of Informatics, King's College London*[*]

[2]*School of Electronic Engineering and Computer Science, Queen Mary University of London*

(Dated: March 29, 2017)

Abstract

Nuclear Quadrupole Resonance (NQR) signal detection can be severely obstructed by interference in real life settings, especially when the interference is strong, nonstationary, and its frequencies are close to that of the NQR signal. A novel algorithm is proposed to effectively remove (or reduce) interference components in the data and facilitate a valid detection of the NQR signal. The proposed method exhibits better performance compared to the previously proposed ETAML and FETAML algorithms, when applied to both simulated and measured data. Importantly, the present algorithm directly operates on the original primary data, without requiring any secondary data (NQR signal-free data) for acquiring prior knowledge of the interference.

[*] This work has been supported by Find a Better Way (FABW) UK, under Project AQUAREOS.

Emails:

weihang.shao@kcl.ac.uk (or picard314@hotmail.com),

jamie.barras@kcl.ac.uk,

k.althoefer@qmul.ac.uk,

panagiotis.kosmas@kcl.ac.uk.

I. INTRODUCTION

Quadrupolar nuclei can resonate when probed by external electromagnetic (EM) waves, leading to an EM response known as the nuclear quadrupole resonance (NQR) signal [1]. Taking advantage of this physical phenomenon, NQR signal detection can be used to identify the presence of substances containing quadrupolar nuclei. As a result, this technique has been applied to problems such as landmine and drug detection, medicine authentication, and oil drilling, etc. [2–4], in order to detect the quadrupolar nuclei which always exist in compounds of the objects of interest (such as the 14N of trinitrotoluen (TNT) in landmines). Several of the NQR signal parameters, such as frequency, signal damping time, and echo decay time depend on the source substance. These parameters can be estimated and used to identify the existence of the NQR signal.

In recent years, algorithms based on least squares estimation or maximum likelihood theory [2, 5, 6] have shown good performance in NQR detection applications. Unfortunately, the NQR signal is usually weak relative to the total received signal. A straightforward strategy to increase the signal-to-noise ratio (SNR) is to repeat measurements and sum up the data, taking advantage of the fact that the NQR signal will add coherently as opposed to radio-frequency (RF) interference and stochastic noise. However, this approach is limited since the time for data collection is usually prohibitively long for real life applications such as humanitarian demining or security checking.

In a traditional NQR data recording system, one needs to let the system fully relax before performing the next data collection. This may take quite a long time, particularly for the detection of substances with long spin-lattice relaxation time. For NQR response signals which decay rapidly with time, the system can record useful data for a very short time and ignore the remaining relaxation time. Based on this observation, a technique called pulsed spin locking sequences [7, 8] or ”echo train” was proposed to improve the method’s efficiency by maintaining the intensity of the NQR signal. Its principle is to echo the NQR signal periodically, so that the NQR signal can almost restore its intensity at each echo except for suffering a weak decay which depends on the quality of the ”echo train” system. The system can therefore record sufficiently long data before full relaxation. This technique has already been a crucial part of most current NQR signal detection systems. The well-known ETAML (echo train approximate maximum-likelihood) algorithm is based on the ”echo train” premise [9].

In NQR signal detection, interference can be a very serious obstruction from detecting the NQR signal of interest. Interference may include effects due to impurities of the NQR sample or

the detection hardware, but is mostly due to the background environment (primarily signals due to radio transmission), and is hard to be shielded against in outdoor measurements. Interference cancelation is therefore never an easy task. Usually, one needs secondary data (NQR signal-free data) to acquire knowledge of the interference, in order to accurately target and cancel the interference in the primary data. A recent algorithm called EPIC has been proved to be very useful for removing interference, in cases where the interference is extremely strong and shares the same frequency with the NQR signal of interest [10]. However, the algorithm requires secondary data which should be strictly synchronous with the primary data and is very difficult to acquire in practice. One way to acquire such data is to use a multi-channel detector [11, 12], where one channel measures the primary data while the others measure the interference and noise at the same time. This multi-channel method can be efficient in cancelling interference, but is a challenging task for real life measurements. For example, channel gains can hardly be the same, and the phase of the data received by different channels may not be equal [13, 14]. To cancel interference from NQR data, a frequency selective method is often used which can be coupled with ETAML algorithm yielding the frequency-selective ETAML (FETAML) algorithm [6, 9]. This method selects the frequency components inside the NQR bands for the data by doing Discrete Fourier transformation (DFT), and excludes the other frequency components.

This paper proposes a novel method to reduce or remove interference in the primary data directly, without using any secondary data. To illustrate our motivation to go beyond frequency selective approaches, we have divided interference into three classes according to their locations relative to the NQR frequency bands, as shown in Fig.1. In this figure, "NQR bands" denote the (very narrow) intervals where the NQR response occurs based on NQR theory (see Eq.(10) and discussion in Section II-B) [15]. Relative to these NQR bands, we can consider three classes of interference based on the proximity of their central frequency to the NQR bands. Class I, which is the farthest and is relatively less important than the other two, can be successfully handled using a frequency selective method [6, 9]. However, when the interference belongs to Class II or III, i.e., in cases where the interference is close to or even coincident with the NQR signal, the components of signal and interference overlap, and the signal is primarily covered by interference. Existing algorithms including frequency selective methods will regard this portion of the interference as a part of the signal, thereby compromising detection performance, as shown in Fig.2. On the contrary, our proposed method can cancel Class II interference, which has a significant portion of its spectrum (but is not centered) inside the NQR bands. Our algorithm does not attempt to cancel Class

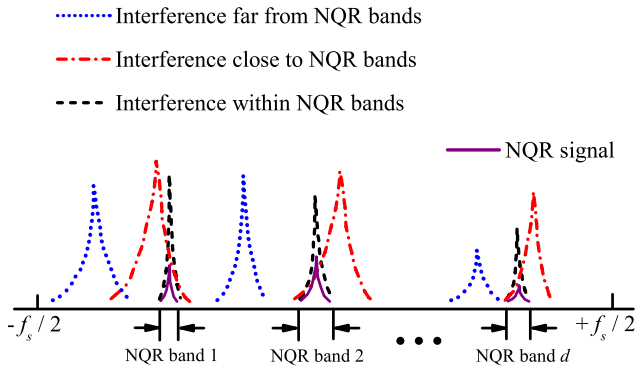

FIG. 1. (Color online) A schematic of the locations of the three classes of interference (in spectrum form) relative to the NQR frequency bands which are defined by the frequency ranges where the NQR signal should appear according to NQR theory [1]. In this graph, f_s denotes the sampling frequency of NQR data, and d is the total number of NQR bands (frequencies) for the NQR signal.

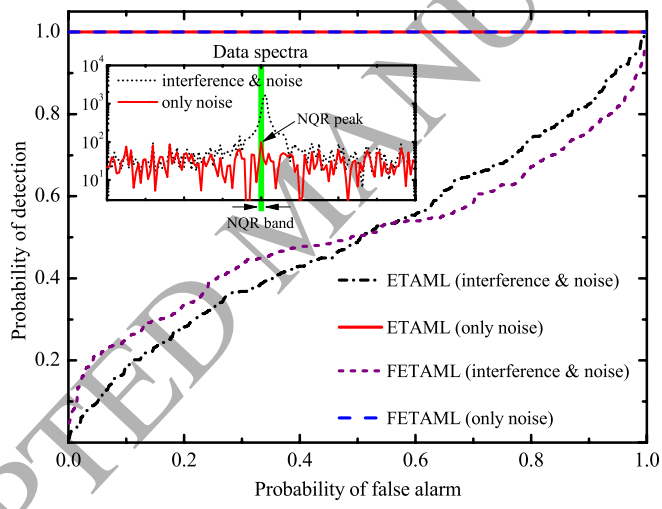

FIG. 2. (Color online) A simple simulation test showing the perfect performance of the well known ETAML and FETAML algorithms on "noise only" NQR signal data, as well as their degradation when NQR data is polluted by a single frequency interference which is very close to NQR band. The NQR signal in this case has only one NQR band (frequency).

III interference, but this class includes uncommon cases of interference which are centered exactly on the resonant frequencies of the NQR response and could be pertinently excluded/shielded in practice. We note that Class II interference not only has a strong sidelobe effect on NQR signal, but may also include strong components in multiple frequencies. The proposed algorithm can ef-

fectively extract and remove Class I and Class II interference from NQR data facilitating a valid NQR signal detection. It is based on operating in two stages, a first stage to cancel interference in the data and then a second stage where the classical ETAML algorithm is applied to the processed data. We have therefore coined the resulting algorithm as interference cancelation ETAML (ICETAML), respectively.

In the next section, we introduce the theory of the new ICETAML algorithm. We then apply the ICETAML algorithm in Section III to both simulated data and experimental data, and compare the results to those obtained by the ETAML and FETAML algorithms. A summary of the main results is given in the last section.

II. THE THEORY OF THE ICETAML ALGORITHM

A. The data model

Considering an echo train detection system, the NQR signal which consists of a total of d components can be accurately modeled for the mth echo as [9]

$$y^m(t) = \sum_{k=1}^{d} \alpha_k e^{-\frac{t+m\mu}{T_k^e}} e^{-\frac{|t-t_{sp}|}{T_k^*} + j2\pi \check{f}_k t}, \tag{1}$$

where t=t_0,...,t_{N-1} is the echo sampling time with the symmetric center to be t_{sp}, μ=2t_{sp} is the echo spacing, and α_k, T_k^e, T_k^*, and $\check{f}_k$ are the amplitude, echo train decay time, damping time, and frequency of the kth component, respectively. Any data z which contains the NQR signal can be divided into three parts: NQR signal y, noise n, and interference r, that is,

$$z^m(t) = y^m(t) + n^m(t) + r^m(t), \tag{2}$$

for the mth echo, where it is assumed that the noise n is white Gaussian and the interference r consists of several discrete single frequency components. If the sampling time for each echo is t=t_0, ..., t_{N-1}, and the total echo number is M in a practical measurement, the entire data z can be rewritten in vector form as

$$\mathbf{Z}_{NM} = \mathbf{Y}_{NM} + \mathbf{N}_{NM} + \mathbf{R}_{NM}, \tag{3}$$

where $\mathbf{N}_{NM}$ and $\mathbf{R}_{NM}$ are the noise and interference parts, respectively. The signal part $\mathbf{Y}_{NM}$ satisfies

$$\mathbf{Y}_{NM} = [y^1(t_0) \quad ... \quad y^1(t_{N-1}) \quad ... \quad y^M(t_0) \quad ... \quad y^M(t_{N-1})]^{\mathrm{T}} = \mathbb{Q}_{NM}\mathbf{A}, \tag{4}$$

where $(.)^{\mathrm{T}}$ denotes the transpose, and $\mathbf{A}$, $\mathbb{Q}_{NM}$ are the amplitude vector and phase matrix, respectively, given by

$$\mathbf{A} = [\alpha_1 \quad \alpha_2 \quad ... \quad \alpha_d]^{\mathrm{T}}, \tag{5}$$

and

$$\mathbb{Q}_{NM} = \begin{pmatrix} \mathbb{P}_1 \\ \mathbb{P}_2 \\ ... \\ \mathbb{P}_M \end{pmatrix}, \quad \mathbb{P}_m = \begin{pmatrix} g(1,1,m) & g(2,1,m) & ... & g(d,1,m) \\ g(1,2,m) & g(2,2,m) & ... & g(d,2,m) \\ ... & ... & ... & ... \\ g(1,N,m) & g(2,N,m) & ... & g(d,N,m) \end{pmatrix}, \tag{6}$$

where $g(k,i,m) = e^{-\frac{(t_{i-1}+m\mu)}{T_k^e} - \frac{|t_{i-1}-t_{sp}|}{T_k^*} + j2\pi\check{f}_k t_{i-1}}$. $\mathbb{Q}_{NM}$ is a matrix of $(N \times M)$ arrays $\times\, d$ columns.

B. Review of the ETAML and FETAML algorithms

The ETAML algorithm [9] estimates the values of the parameters α_k, $\check{f}_k$, T_k^*, and T_k^e, based on maximum-likelihood theory. To do so, the amplitudes vector $\mathbf{A}$ in Eq. (5) is estimated as

$$\hat{\mathbf{A}} = \mathbb{Q}_{NM}^{\dagger}\mathbf{Z}_{NM}, \tag{7}$$

where $(.)^{\dagger}$ denotes the Moore-Penrose pseudo-inverse. Then, the likelihood function for $\check{f}_k$, T_k^*, and T_k^e can be written as

$$L(\check{f}_k, T_k^*, T_k^e) = \mathbf{Z}_{NM}^{\mathrm{H}}\mathbb{Q}_{NM}\mathbb{Q}_{NM}^{\dagger}\mathbf{Z}_{NM}, \tag{8}$$

where $(.)^{\mathrm{H}}$ denotes the conjugate transpose. As $\hat{\alpha_k}$ are functions of $\check{f}_k$, T_k^*, and T_k^e, estimating the parameters α_k, $\check{f}_k$, T_k^*, and T_k^e is equal to finding the $\check{f}_k$, T_k^*, and T_k^e values which satisfy $|L|=\max(|L|)$.

The search ranges for $\check{f}_k$, T_k^*, and T_k^e should respectively cover all the possible values of $\check{f}_k$, T_k^*, and T_k^e under immediate environment conditions based on knowledge of NQR theory [15]. In particular,

$$\check{f}_k = a_k - b_k Temp, \tag{9}$$

where $Temp$ is the environment temperature, and a_k and b_k are coefficients which are determined by the studied substance, respectively. If $Temp$ has an average value $Temp_0$ with an uncertainty ΔT, we have

$$\check{f}_k \in [\check{f}_{k0} - b_k\Delta T, \check{f}_{k0} + b_k\Delta T], \quad \check{f}_{k0} = a_k - b_k Temp_0, \tag{10}$$

which are called NQR bands and are used as the search range for $\check{f}_k$ in this paper.

Once the values of parameters ($\check{f}_k$, T_k^*, T_k^e) are estimated, they can be substituted into the ETAML test statistic [16]

$$T(\mathbf{Z}_{NM}) = (2NM-1)\frac{\mathbf{Z}_{NM}^{\mathrm{H}}\mathbb{Q}_{NM}\mathbb{Q}_{NM}^{\dagger}\mathbf{Z}_{NM}}{\mathbf{Z}_{NM}^{\mathrm{H}}\mathbf{Z}_{NM} - \mathbf{Z}_{NM}^{\mathrm{H}}\mathbb{Q}_{NM}\mathbb{Q}_{NM}^{\dagger}\mathbf{Z}_{NM}}. \tag{11}$$

By predetermining a threshold value γ, the NQR signal is deemed present if and only if $T(\mathbf{Z}_{NM})>\gamma$, and otherwise not. To reduce false alarms, an effective detection algorithm should produce large $T(\mathbf{Z}_{NM})$ values when the NQR signal is present, and small ones otherwise.

The ETAML algorithm is very useful when interference in the data is limited. However, its performance degrades if interference becomes very strong, non-stationary, and is very close to the NQR signal's frequency. To overcome some of these limitations, a variant of the ETAML algorithm known as FETAML has been reported [9]. The FETAML algorithm is a combination of ETAML and the frequency selective method.

As mentioned in the Introduction, the frequency selective method can cancel Class I interference (see Fig. 1) by dividing the NQR bands in a vector of J subbands, $[f_{s1} \quad f_{s2} \quad ... \quad f_{sJ}]$. Performing a DFT for $\mathbf{Z}_{NM}$ and $\mathbb{Q}_{NM}$ yields

$$\left(\widetilde{\mathbf{Z}}_{JM}, \widetilde{\mathbb{Q}}_{JM}\right) = \begin{pmatrix} \mathbb{V}_J & & \\ & \mathbb{V}_J & \\ & & .. \\ & & \mathbb{V}_J \end{pmatrix} (\mathbf{Z}_{NM}, \mathbb{Q}_{NM}), \quad \mathbb{V}_J = \begin{pmatrix} 1 & e^{-j2\pi f_{s1}/f_s} & .. & e^{-j2\pi(N-1)f_{s1}/f_s} \\ 1 & e^{-j2\pi f_{s2}/f_s} & .. & e^{-j2\pi(N-1)f_{s2}/f_s} \\ .. & .. & .. & .. \\ 1 & e^{-j2\pi f_{sJ}/f_s} & .. & e^{-j2\pi(N-1)f_{sJ}/f_s} \end{pmatrix}, \tag{12}$$

where f_s is the sampling frequency. By combining this method with ETAML, Eqs.(8) and (11) become,

$$\begin{aligned} \widetilde{L}(\omega_k, T_k^*, T_k^e) &= \widetilde{\mathbf{Z}}_{JM}^{\mathrm{H}}\widetilde{\mathbb{Q}}_{JM}\widetilde{\mathbb{Q}}_{JM}^{\dagger}\widetilde{\mathbf{Z}}_{JM}, \\ \widetilde{T}(\widetilde{\mathbf{Z}}_{JM}) &= (2JM-1)\frac{\widetilde{\mathbf{Z}}_{JM}^{\mathrm{H}}\widetilde{\mathbb{Q}}_{JM}\widetilde{\mathbb{Q}}_{JM}^{\dagger}\widetilde{\mathbf{Z}}_{JM}}{\widetilde{\mathbf{Z}}_{JM}^{\mathrm{H}}\widetilde{\mathbf{Z}}_{JM} - \widetilde{\mathbf{Z}}_{JM}^{\mathrm{H}}\widetilde{\mathbb{Q}}_{JM}\widetilde{\mathbb{Q}}_{JM}^{\dagger}\widetilde{\mathbf{Z}}_{JM}}. \end{aligned} \tag{13}$$

C. Interference cancelation by the ICETAML algorithm

As argued in the Introduction, it is critical to deal with Class II interference components, which are centered outside but very close to the NQR bands. For this type of interference, which has significant portion of its spectrum "leaking" into the NQR bands and concealing the target response, our algorithm operates in the frequency interval "$\left[-\frac{f_s}{2}, \frac{f_s}{2}\right]$-NQR bands" (see Fig. 1), marked as

C_I, where $\left[-\frac{f_s}{2}, \frac{f_s}{2}\right]$ should be the entire frequency band of complex digital data sampled at frequency f_s. To cancel the interference, the ICETAML algorithm first divides the data vector $\mathbf{Z}_{NM}$ into M parts, with each part containing a single echo, and then performs interference cancelation for each part separately. The entire frequency band $\left[-\frac{f_s}{2}, \frac{f_s}{2}\right]$, where f_s is the sampling frequency, is discretized to be $[f_1, f_2, ..., f_K]$. Thus, the mth part $\mathbf{Z}_m$ is approximated as

$$\mathbf{Z}_m \simeq \sum_{k=1}^{K} \beta_k e^{j2\pi f_k \mathbf{t}}, \quad \mathbf{t} = [t_0, t_1, ..., t_{N-1}]^{\mathrm{T}}, \tag{14}$$

where β_k and f_k denote the complex amplitude and the frequency of the kth component, respectively.

Our purpose is then to pick out frequency components with strong interference and remove them from $\mathbf{Z}_m$. For any frequency $f_k \in C_I$, the cost function for this frequency component can be written as

$$C(f) = \min_{\beta} ||\mathbf{Z} - \mathbf{F}(f)\beta||_2^2 = ||\mathbf{Z} - \mathbf{F}(f)\mathbf{F}^{\dagger}(f)\mathbf{Z}||_2^2, \tag{15}$$

where $\mathbf{F}(f_k)=[e^{j2\pi f_k t_0}, ..., e^{j2\pi f_k t_{N-1}}]^{\mathrm{T}}$ is the Fourier vector for frequency f_k. The smallest $C^{(1)}$, marked as $C^{(1)}(f_{m1})$, should be corresponding to the strongest interference. This interference can be removed from $\mathbf{Z}_m$ as

$$\mathbf{Z}_m^{(1)} = \mathbf{Z}_m - \mathbf{F}(f_{m1})\mathbf{F}^{\dagger}(f_{m1})\mathbf{Z}_m. \tag{16}$$

As $Z_m^{(1)}$ is acquired, it is necessary to check if there are other strong remaining interference components. We herein define a threshold $Th(\mathbf{Z}_m)=2S(\mathbf{Z}_m)$, where

$$S(\mathbf{Z}_m) = \frac{1}{N} \sum_{k=0}^{N-1} \left| \sum_{n=0}^{N-1} \mathbf{Z}_m(n) e^{-j2\pi \frac{kn}{N}} \right|, \tag{17}$$

denotes the average spectrum intensity of the $\mathbf{Z}_m$. The ICETAML/ICFETAML algorithm cancels all the interference frequency components whose spectrum intensities are higher than $Th(\mathbf{Z}_m)$. That is to say, if there is $f_k \in C_I$ which satisfies

$$\left| \sum_{n=0}^{N-1} \mathbf{Z}_m^{(1)}(n) e^{-j2\pi \frac{nf_k}{f_s}} \right| > Th(\mathbf{Z}_m), \tag{18}$$

then these strong interference components must be removed. Then, finding the minimal value of the new cost function

$$C^{(2)}(f_k) = ||\mathbf{Z}_m^{(1)} - \mathbf{F}(f_k)\mathbf{F}^{\dagger}(f_k)\mathbf{Z}_m^{(1)}||_2^2, \tag{19}$$

yields the corresponding frequency f_{m2} which corresponds to one of the dominant interference frequencies. To remove the interference components of f_{m1} and f_{m2} from $\mathbf{Z}_m$ together, we have

$$\mathbf{Z}_m^{(2)} = \mathbf{Z}_m - [\mathbf{F}(f_{m1}) \quad \mathbf{F}(f_{m2})][\mathbf{F}(f_{m1}) \quad \mathbf{F}(f_{m2})]^{\dagger}\mathbf{Z}_m. \tag{20}$$

where $[\mathbf{F}(f_{m1}) \quad \mathbf{F}(f_{m2})]$ is formed by combining the vectors to the corresponding matrix.

Table: Iteration

i=1;
while $\left(\left|\sum_{n=0}^{N-1} \mathbf{Z}_m^{(i)}(n)e^{-j2\pi\frac{nf_k}{f_s}}\right| > Th(\mathbf{Z}_m)\right)$
  i=i+1;
  $C^{(i)}(f_{mi}) = \min_{f_k}\left[\|\mathbf{Z}_m^{(i-1)} - \mathbf{F}(f_k)\mathbf{F}^{\dagger}(f_k)\mathbf{Z}_m^{(i-1)}\|_2^2\right]$;
  $\mathbf{Z}_m^{(i)} = \mathbf{Z}_m - [\mathbf{F}(f_{m1}) \quad ... \quad \mathbf{F}(f_{mi})][\mathbf{F}(f_{m1}) \quad ... \quad \mathbf{F}(f_{mi})]^{\dagger}\mathbf{Z}_m$;
end

By applying this process iteratively, as shown in "Table: Iteration", the main interference components $(f_{m1}, f_{m2}, ..., f_{ml})$, $i = 1, 2, ..., l$, can be picked out by satisfying,

$$C^{(i)}(f_{mi}) = \min_{f_k}\left[\|\mathbf{Z}_m^{(i-1)} - \mathbf{F}(f_k)\mathbf{F}^{\dagger}(f_k)\mathbf{Z}_m^{(i-1)}\|_2^2\right], \tag{21}$$

and the ultimate interference-canceled data $\mathbf{Z}_m^{(l)}$

$$\mathbf{Z}_m^{(l)} = \mathbf{Z}_m - [\mathbf{F}(f_{m1}) \quad \mathbf{F}(f_{m2}) \quad ... \quad \mathbf{F}(f_{ml})][\mathbf{F}(f_{m1}) \quad \mathbf{F}(f_{m2}) \quad ... \quad \mathbf{F}(f_{ml})]^{\dagger}\mathbf{Z}_m, \tag{22}$$

is acquired, which satisfies $\left|\sum_{n=0}^{N-1} \mathbf{Z}_m^{(l)}(n)e^{-j2\pi\frac{nf_k}{f_s}}\right| \leq Th(\mathbf{Z}_m)$, for $\forall f_k \in C_1$. The physical significance of Eq. (22) is explained in the Appendix. The value of $Th(\mathbf{Z}_m)$ is set a little larger than the maximum noise spectrum intensity. According to our numerical tests, $2S(\mathbf{Z}_m)$ is a suitable choice for $Th(\mathbf{Z}_m)$ if noise level is not very high (or very low), see for example Fig. 3. Anyway, we can determine $Th(\mathbf{Z}_m)$ after scanning the exact spectrum of $\mathbf{Z}_m$. This threshold setting ensures that the proposed algorithm cancels the dominant part of interference which is beyond the noise level, so that residual interference after cancellation can be treated as noise signal. The iterative process is thus terminated when the remaining interference and noise have comparable intensity, and then the ICETAML algorithm converts to the classical ETAML algorithm applied to the remaining "interference-free" data. In principle, the proposed interference cancelation method can also couple with FETAML. We accordingly call this combination "ICFETAML". It is worth investigating

then whether ICFETAML, by utilizing the frequency selective method to cancel the remaining interference, performs better than ICETAML. The performance of both ICETAML and ICFETAML will be discussed in the following analysis of the algorithm's performance.

III. THE PERFORMANCE OF THE ICETAML ALGORITHM

After a brief introduction to our NQR detection testbed and data acquisition method, this section presents results for both simulated and experimental data which validate the ICETAML algorithm and demonstrate its superior performance relative to the previously proposed ETAML and FETAML algorithms.

A. Introduction to our NQR data

Our testbed examines detection of the ^{14}N NQR signal due to sodium nitrite ($NaNO_2$). To acquire experimental data, we prepared two sealed plastic boxes which were both filled with silicone oil and were buried under soil separately. All conditions are the same between the two boxes except for the presence of a piece of solid $NaNO_2$, which is suspended in the silicone oil in only one of the boxes. Signal data in echo train mode is recorded by a spectrometer with a sampling frequency $f_s = \frac{1}{16\mu s}$. Two data sets are acquired for each run/record, one with and one without the NQR signal. The data signal comprises of N=128 sampling points (complex numbers) per M=32 echoes.

For the studied substance under our lab conditions, the NQR signal has only one resonant frequency $\check{f}\simeq$1.0365MHz, with the parameters T^* and T^e in Eq. (1) satisfying $T^*\simeq$1.74ms, and $T^e\simeq$88ms, respectively. In addition, b in Eq. (9) is 600Hz/Kelvin, and the lab temperature uncertainty ΔT is about 0.8Kelvin. The real frequency band of the data is $\left[f_c - \frac{f_s}{2}, f_c + \frac{f_s}{2}\right]$, where f_c denotes the frequency center of our signal modulation. The algorithm can effectively treat the frequency band of the recorded data as $\left[-\frac{f_s}{2}, \frac{f_s}{2}\right]$. Particularly, we let $f_c \simeq \check{f}$, so that the modulated NQR band is $[-b\Delta T, +b\Delta T]$ (see Eq. (10)).

In our calculations, we set the search step for the NQR band as $\frac{b\Delta T}{10}$ ($\simeq$48Hz), which is also used as the grid step size of $[f_{s1} \quad f_{s2} \quad ... \quad f_{sJ}]$ for calculating Eq. (12). The search ranges of T^* and T^e are set to be $[1.74\text{ms} \times 0.01, 1.74\text{ms} \times 10.01]$ and $[88\text{ms} \times 0.01, 88\text{ms} \times 10.01]$ which already cover all the possible T^* and T^e values under our lab conditions according to NQR theory [15],

with the search steps being $\frac{1.74\text{ms}}{100}$ and $\frac{88\text{ms}}{100}$, respectively. Moreover, the search step for the C_I is set to be $\frac{f_s}{10N}$ ($\simeq$48Hz) in the ICETAML and ICFETAML.

We note that both IC and ETAML/FETAML steps of the combined ICETAML/ICFETAML algorithms are based on optimization searches that are computationally intensive, with ETAML/FETAML requiring a multi-parameter search. For all the cases in this paper, the search steps for both IC and ETAML/FETAML are constant and small enough the ensure accurate results. In practice, this strategy may lead to long calculating times, and thus advanced optimum search methods such as the conjugate gradient method [17] should be applied to ensure accuracy and reasonable computational cost.

Based on the above physical considerations, we have generated simulated data which models possible experimental data with different types of interference. We present first results from these datasets, followed by application to experimental data acquired in our lab.

B. Simulated data test I: stationary interference case

We created a simulated dataset, which consists of 500 Monte Carlo runs. In this set, the amplitude of the NQR signal is set as α=1, whereas the noise is zero-mean Gaussian white noise with variance D=2.25. The signal to noise ratio (SNR) can be calculated as,

$$\text{SNR} = 20\lg\left(\frac{\pi}{4}\cdot\frac{\alpha^2}{D}\right), \tag{23}$$

and is equal to -9dB which is very close to the SNR of our experimental data. The simulated interference contains nine stationary components.

$$r(t) = \sum_{i=1}^{9} 8e^{j2\pi f_i t + j\varphi_i}, \quad Nf_i/f_s = 1.5, 1.6, 1.7, 2.0, 2.1, 2.3, 2.8, 3.0, 3.2,$$

where all the initial phases φ_i vary randomly among the runs. The nine components are all very close to the NQR band. In particular, by defining df=f_s/N ($\simeq b\Delta T$) to be the resolution of spectrum, the NQR band is approximately [−df, +df], and the distance between interference and NQR band is only 1.5df (frequency of the first component)-df=0.5df. In order to test the efficiency of our cancellation method, the first echo $\mathbf{Z}_1$ of a data containing NQR signal is shown in Fig.3. It is seen that the ICETAML/ICFETAML algorithm is useful for removing the interference and it almost restores the data to be at the "NQR signal + white noise" level. As a result, the receiver

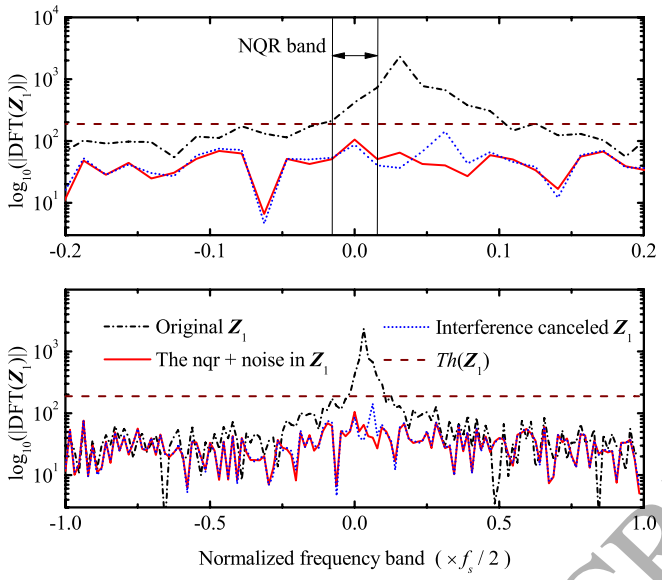

FIG. 3. (Color online) The performance of the present interference cancelation method for the simulated "Data Test I". "DFT" denotes Discrete Fourier transformation. The upper subplot is zoomed into the interval around the NQR band. $\mathbf{Z}_1$ is a part of simulated data which contains NQR signal, as well as strong and stationary interference whose frequencies are all very close to the NQR signal frequency. For this dataset, SNR=-9dB. All the interference frequency components with intensities larger than the threshold $Th(\mathbf{Z}_1)$ (where $Th(\mathbf{Z}_1)/2$ is the average spectrum intensity of the $\mathbf{Z}_1$) are cancelled.

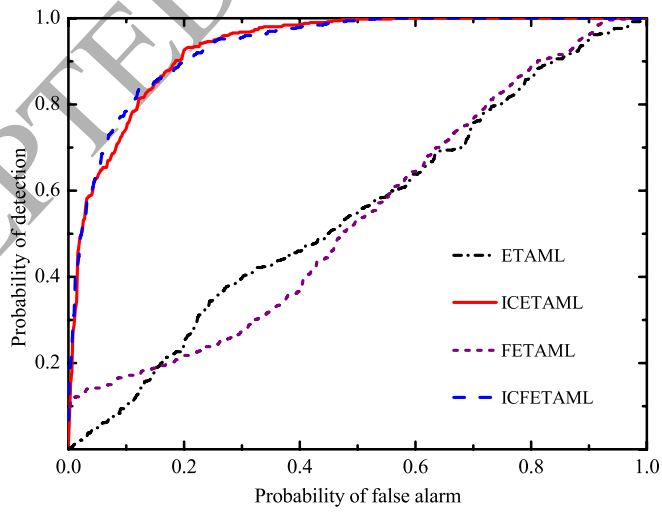

FIG. 4. (Color online) The ROC curves obtained by ICETAML and ICFETAML algorithms, and the previously reported ETAML and FETAML algorithms for the simulated "Data Test I".

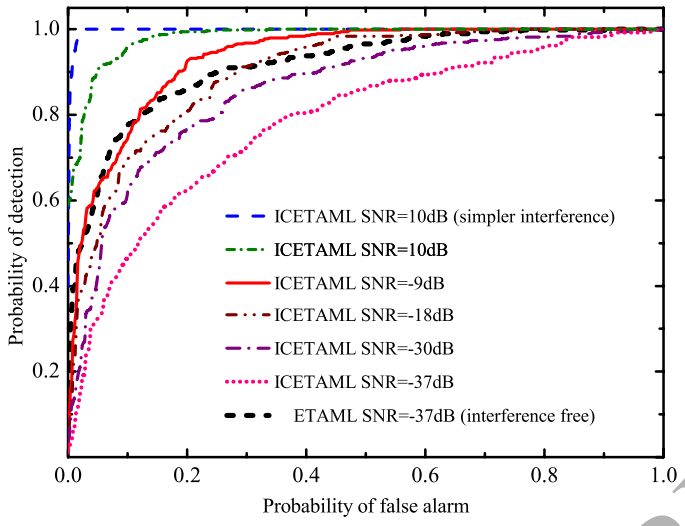

FIG. 5. (Color online) The ROC curves obtained by ICETAML for the simulated "Data Test I" of different SNRs.

operating characteristic (ROC) curves of the ICETAML and ICFETAML algorithms clearly outerperform those of the ETAML and FETAML algorithms, as shown in Fig.4. In particular, Figure 4 demonstrates that strong interference causes the ETAML to perform poorly, even when combined with the frequency selective method (FETAML). On the contrary, the ICETAML and ICFETAML algorithms are very effective in cancelling interference leading to accurate NQR detection. We note that the combination of the frequency selective method and the proposed interference cancelation method has little impact in this case, as evidenced by the similarity in the ROC curves of the ICFETAML and ICETAML algorithms.

In addition, it is worth analyzing the influence of SNR on ICETAML's performance. For this purpose, let's first assume the ETAML algorithm being applied to interference-free data, and consider SNR_0 to be the minimal SNR for a valid detection by ETAML. If data is polluted by interference, a valid detection by ICETAML would require (in the best case scenario) an SNR no smaller than SNR_0, since ICETAML transforms to ETAML after interference cancellation. In practice, a residual interference after applying Eq. (22) will be presented in the signal, and will be added to the original noise, leading to an SNR lower than SNR_0. The stronger or the more complicated the interference is, the larger is this residual, and the higher is the SNR required for a valid detection by ICETAML. To study further the impact of noise, we have plotted ROC curves for different SNR values in Fig.(5). Naturally, performance degrades as the SNR decreases. The effect of the remaining interference on SNR is illustrated by comparing performance when ICETAML is

applied (for the same SNR=10dB) to the original and a simplified interference dataset obtained by deleting components Nf_i/f_s=1.7, 2.0, 3.0, and 3.2 (upper dash vs. short dash dotted line in Fig.5). The plot also illustrates that the impact of non-perfect interference cancellation becomes stronger for very low SNRs (e.g. -37dB), for which an interference-free ETAML exhibits superior performance than the ICETAML algorithm.

C. Simulated data test II: nonstationary interference case

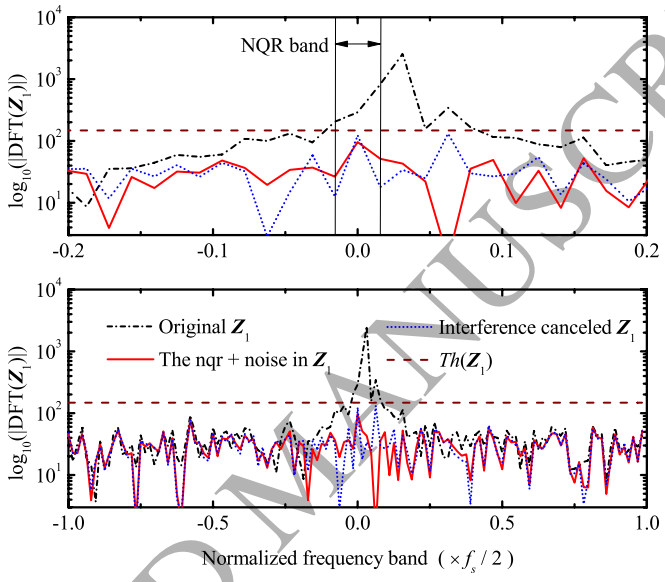

FIG. 6. (Color online) The performance of the present interference cancelation method for the simulated "Data Test II". "DFT" denotes Discrete Fourier transformation. The upper subplot is zoomed into the interval around the NQR band. $\mathbf{Z}_1$ is a part of simulated data which contains NQR signal, as well as strong and nonstationary interference whose frequencies are all very close to the NQR signal frequency. For this dataset, SNR=-9dB. All the interference frequency components with intensities larger than the threshold $Th(\mathbf{Z}_1)/2$ (where $Th(\mathbf{Z}_1)/2$ is the average spectrum intensity of $Th(\mathbf{Z}_1)/2$) are cancelled.

"Nonstationary" interference occurs if its frequency, phase, or amplitude varies with time. Detection in the presence of nonstationary interference is much more complicated, as a general Fourier transformation can only infer the average spectrum of a nonstationary signal within a certain time interval but is unable to capture its true time-varying spectrum. To test performance of the ICETAML algorithm for nonstationary interference, we replaced two stationary interference

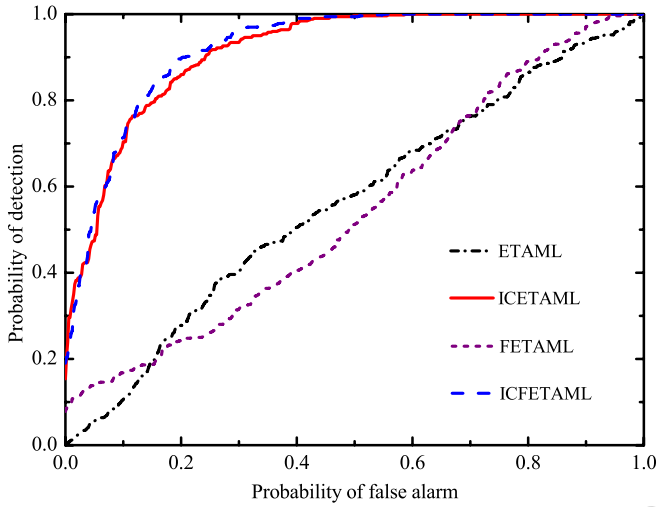

FIG. 7. (Color online) The ROC curves obtained by ICETAML and ICFETAML algorithms, and the previously reported ETAML and FETAML algorithms for the simulated "Data Test II".

components with two nonstationary ones in the simulated data of the former subsection. The simulated interference is written as

$$r(t) = \sum_{i=1}^{7} 8e^{j2\pi f_i t + j\varphi_i} + \sum_{i=1}^{2} 8e^{j2\pi f_{\text{non}i} t + j\varphi_i}, \quad Nf_i/f_s = 1.6, 1.7, 2.0, 2.1, 2.3, 3.0, 3.2,$$

$$f_{\text{non}i} = (1.5 + 1.0t \times f_s/(NM)) \times f_s/N, \quad (2.8 - 0.5t \times f_s/(NM)) \times f_s/N,$$

where all the initial phases φ_i vary randomly among the runs. The interference cancelation result is plotted in Fig.6. We see that, although the ICETAML algorithm cancels nonstationary interference according to its average spectrum, it exhibits good robustness with respect to the time-varying interference characteristics. The related ROC curves are shown in Fig.7. Compared to those in Fig.4, the ICETAML's performance slightly deteriorates in this case, which confirms that detection in the presence of nonstationary interference is more challenging than in the case of stationary interference. As for the previous case, ICFETAML and ICETAML have again similar performance.

D. Simulated data test III: "remote interference" case

A third scenario which merits investigation involves cancellation of "remote interference" on the data, that is, interference with spectrum that is at some distance from the NQR signal (the "Class I" interference in Fig. 1). In particular, we are interested in investigating whether the

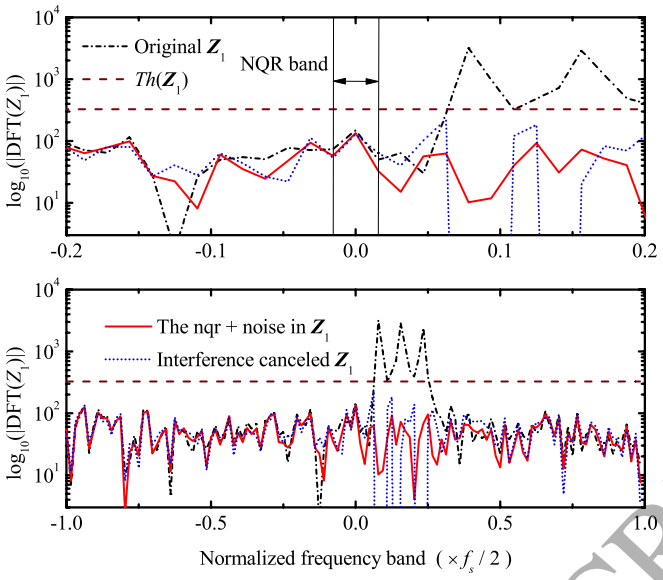

FIG. 8. (Color online) The performance of the present interference cancelation method for the simulated "Data Test III". "DFT" denotes Discrete Fourier transformation. The upper subplot is zoomed into the interval around the NQR band. $\mathbf{Z}_1$ is a part of simulated data which contains NQR signal, as well as strong and nonstationary interference with distant frequencies from the NQR band. For this dataset, SNR=-9dB. All the interference frequency components with intensities larger than the threshold $Th(\mathbf{Z}_1)/2$ (where $Th(\mathbf{Z}_1)/2$ is the average spectrum intensity of $Th(\mathbf{Z}_1)/2$) are cancelled.

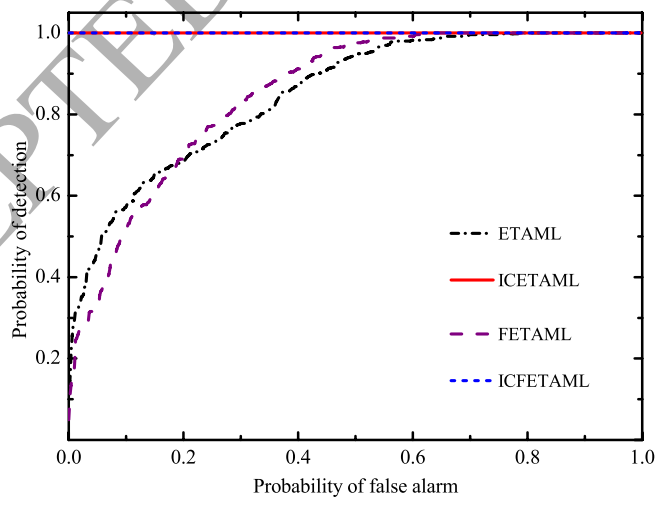

FIG. 9. (Color online) The ROC curves obtained by ICETAML and ICFETAML algorithms, and the previously reported ETAML and FETAML algorithms for the simulated "Data Test III".

frequency selective method can cancel this type of interference if there is weak overlap between the NQR signal and the interference spectrum. To this end, we have simulated new interference as

$$r(t) = \sum_{i=1}^{15} 10e^{j2\pi f_i t + j\varphi_i} + \sum_{i=1}^{3} 10e^{j2\pi f_{\mathrm{non}i} t + j\varphi_i},$$

$$Nf_i/f_s = 4.7, 4.8, 4.9, 5, 5.1, 9.8, 9.9, 10, 10.1, 10.2, 14.9, 15, 15.1, 15.2, 15.3,$$

$$f_{\mathrm{non}i} = (5.7 - 0.8t \times f_s/(NM)) \times f_s/N, \quad (10.5 - 0.6t \times f_s/(NM)) \times f_s/N,$$
$$(14.4 + 0.7t \times f_s/(NM)) \times f_s/N,$$

where all the initial phases φ_i vary randomly among the runs. Performance in this case is shown in Fig.8, which confirms that the overlap with the NQR signal is weak and that the ICETAML and ICFETAML algorithms manage to cancel this interference. It is evident from the ROC curves in Fig.9 that the frequency selective method fails in this case, while the ICETAML and ICFETAML algorithms output very good results. These results suggest further advantages of our algorithm relative to simple frequency selective methods, which cannot deal with all kinds of "Class I" interference.

E. Simulated data test IV: interference spread in a wide range of frequencies

The aforementioned three simulating cases have already confirmed the superior performance of the ICETAML algorithm relative to previous methods. An additional simulating case is present here in order to test if ICETAML works well for situations where strong interference of Classes I and II are both present in the signal. The simulated interference in this case has a wide range of frequencies,

$$r(t) = \sum_{i=1}^{9} 5e^{j2\pi f_i t + j\varphi_i} + \sum_{i=1}^{7} 5e^{j2\pi f_{\mathrm{non}i} t + j\varphi_i}, \quad Nf_i/f_s = 1.5, 1.6, 1.7, 2.0, 2.1, 2.3, 2.8, 3.0, 3.2,$$

$$f_{\mathrm{non}i} = (1.5 + 1.0t \times f_s/(NM)) \times f_s/N, \quad (4 - 0.3t \times f_s/(NM)) \times f_s/N,$$
$$(5.7 - 0.8t \times f_s/(NM)) \times f_s/N, \quad (14.4 + 0.3t \times f_s/(NM)) \times f_s/N$$
$$(25.5 + 0.3t \times f_s/(NM)) \times f_s/N, \quad (-13 - 0.7t \times f_s/(NM)) \times f_s/N$$
$$(-25 - 0.9t \times f_s/(NM)) \times f_s/N,$$

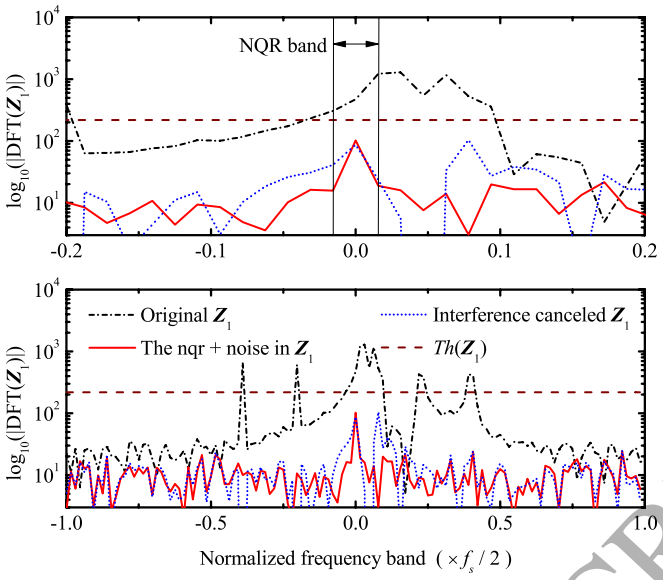

FIG. 10. (Color online) The performance of the present interference cancelation method "Data Test IV". "DFT" denotes Discrete Fourier transformation. The upper subplot is zoomed into the interval around the NQR band. $\mathbf{Z}_1$ is a part of simulated data which contains NQR signal, as well as strong and stationary (or nonstationary) interference with wide range frequencies. For this dataset, SNR=10dB. All the interference frequency components with intensities larger than the threshold $Th(\mathbf{Z}_1)/2$ (where $Th(\mathbf{Z}_1)/2$ is the average spectrum intensity of $Th(\mathbf{Z}_1)/2$) are cancelled.

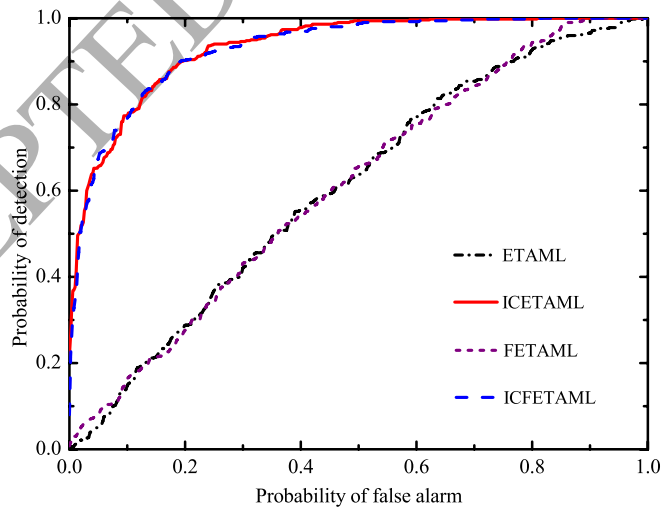

FIG. 11. (Color online) The ROC curves obtained by ICETAML and ICFETAML algorithms, and the previously reported ETAML and FETAML algorithms for the simulated "Data Test IV".

where all the initial phases φ_i vary randomly among the runs. A higher SNR is needed for effectively cancelling this complicated interference, based on the analysis of the SNR's influence on ICETAML's performance at the end of Section III-B. We let the noise variance D in this case be 0.25, which leads to SNR=10dB (see Eq. (23)). The results of interference cancelation and ROC curves are in Fig.10 and Fig.11, respectively, which suggest that the proposed algorithm can be applied to NQR data polluted by general strong and complicated interference with a wide range of frequencies. Moreover, we have performed additional numerical studies which have confirmed that the proposed ICETAML algorithm can successfully cancel interference with more frequency components.

F. Experimental data test

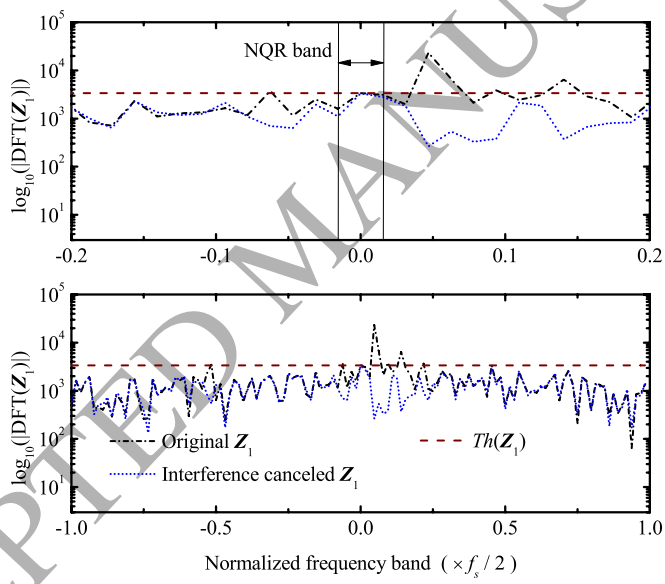

FIG. 12. (Color online) The performance of the present interference cancelation method for our experimental dataset. "DFT" denotes Discrete Fourier transformation. The upper subplot is zoomed into the interval around the NQR band. $\mathbf{Z}_1$ is a part of experimental data which contains the NQR signal, as well as strong and nonstationary interference with frequencies mainly located very close to the NQR signal frequency. The SNR is about -10dB for the experimental data. All the interference frequency components with intensities larger than the threshold $Th(\mathbf{Z}_1)/2$ (where $Th(\mathbf{Z}_1)/2$ is the average spectrum intensity of $Th(\mathbf{Z}_1)/2$) are cancelled.

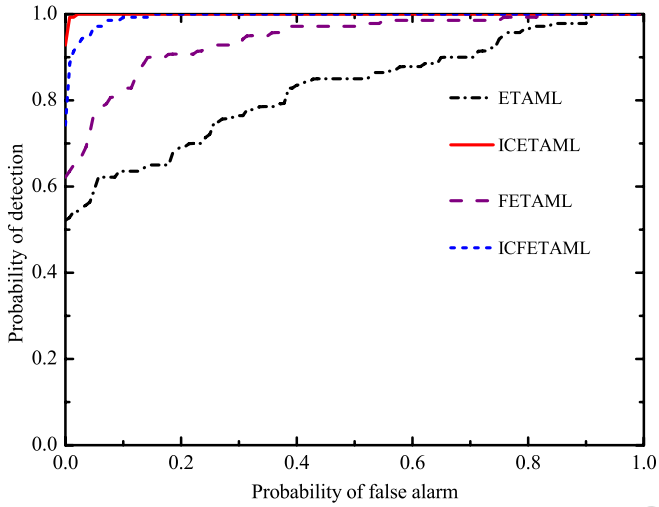

FIG. 13. (Color online) The ROC curves obtained by ICETAML and ICFETAML algorithms, and the previously reported ETAML and FETAML algorithms for the experimental dataset of Fig.12.

We acquired experimental data consisting of a total of 140 runs. In our lab where our experiments were performed, background electrical instruments/appliances and mobile signals can act as interference to NQR detection, but other significant sources of interference such as radio signals are at lower level than in outdoor experimental settings. Therefore, in order to generate additional interference that would account for more challenging experimental conditions, we generated an EM wave with a sinusoidal envelope line and a slow time-varying frequency being located very close to NQR band. Nearby electrical instruments/appliances and mobile signals in the background were also present in the experimental data, but were relatively weak and located far from NQR band (please see Fig.12 for more details). The interference cancelation result and ROC curves are displayed in Figs.12 and 13, respectively. It is clearly shown that the present interference cancelation algorithm is effective, and successfully reduces the interference effect. From the ROC curves, the advantage of the ICETAML and ICFETAML over the ETAML and FETAML algorithms is also evident. These preliminary experimental results suggest that the ICETAML algorithm can improve significantly NQR detection in real-life settings.

Finally, the ICFETAML does not have again distinct advantages over ICETAML, similar to our simulated results. This means that our proposed method of cancelling interference is robust and effective without the need to combine it with a frequency selective method.

IV. CONCLUSION

This paper presents a novel interference cancelation method which can enhance NQR signal detection. The method can be coupled with the classical ETAML algorithm resulting in the formulation of the so-called ICETAML algorithm. When data are severely polluted by strong interference, the ETAML algorithm and its modified version FETAML (which is a combination of ETAML and a frequency selective interference cancelation method) degrades, while the ICETAML algorithm can effectively cancel interference and improve NQR signal detection significantly. In particular, the paper's results show that the ICETAML algorithm exhibits excellent performance when applied to simulated data or experimental data, even in cases where interference is very strong, nonstationary, and has frequencies which are very close to that of NQR signal.

V. APPENDIX

To discuss the physical significance of Eq. (22), we start by noting that,

$$\mathbb{G}^{\dagger} = [\mathbf{F}(f_{m1}) \quad \mathbf{F}(f_{m2}) \quad ... \quad \mathbf{F}(f_{ml})]^{\dagger} = [\mathbf{F}_1^{\mathrm{T}} \quad \mathbf{F}_2^{\mathrm{T}} \quad ... \quad \mathbf{F}_l^{\mathrm{T}}]^{\mathrm{T}}, \tag{24}$$

where $\mathbf{F}_1$, $\mathbf{F}_2$, ...,$\mathbf{F}_l$ are $1\times N$ vectors which should satisfy

$$\mathbf{F}_i\mathbf{F}(f_{mj}) = \delta_{ij}, \tag{25}$$

where δ_{ij} is 1 if i=j, or 0 otherwise. Thus, we have

$$\mathbf{Z}_m^{(l)} = \left(\mathbb{I} - \sum_{i=1}^{l} \mathbf{F}(f_{mi})\mathbf{F}_i\right)\mathbf{Z}_m, \tag{26}$$

where $\mathbb{I}$ is the unit matrix. Three main conclusions can be derived: (1). The extracted interference $\mathbb{G}\mathbb{G}^{\dagger}\mathbf{Z}_m$ is orthogonal with $\mathbf{Z}_m^{(l)}$, the rest part of $\mathbf{Z}_m$.

$$\left(\mathbb{G}\mathbb{G}^{\dagger}\mathbf{Z}_m\right)^{\mathrm{H}}\left(\mathbf{Z}_m - \mathbb{G}\mathbb{G}^{\dagger}\mathbf{Z}_m\right) = \mathbf{Z}_m^{\mathrm{H}}\mathbb{G}\mathbb{G}^{\dagger}\left(\mathbb{I} - \mathbb{G}\mathbb{G}^{\dagger}\right)\mathbf{Z}_m = 0. \tag{27}$$

(2). All the frequency components of the extracted interference components, $\mathbf{V}_i$=$\mathbf{F}(f_{mi})\mathbf{F}_i\mathbf{Z}_m$, i=1,2,...,l, are approximately orthogonal with each other. Assuming the sampling is uniform, that is, t_i=$(i-1)dt$, i=1,2,...,N, where dt is the time interval of sampling, we have

$$\mathbf{F}(f_{mi})^{\mathrm{H}}\mathbf{F}(f_{mj}) = \sum_{k=1}^{N} e^{-j2\pi(f_{mi}-f_{mj})(k-1)dt} = \frac{e^{-j\pi(f_{mi}-f_{mj})Ndt}}{e^{-j\pi(f_{mi}-f_{mj})dt}}\frac{\sin(\pi(f_{mi}-f_{mj})Ndt)}{\sin(\pi(f_{mi}-f_{mj})dt)}, \tag{28}$$

so that

$$\begin{aligned} \mathbf{F}(f_{mi})^{\mathrm{H}}\mathbf{F}(f_{mi}) &= N, \quad i = 1, 2, ..., l, \\ \left|\mathbf{F}(f_{mi})^{\mathrm{H}}\mathbf{F}(f_{mj})\right| &\ll N, \quad i \neq j. \end{aligned} \tag{29}$$

According to Eq.(29), it can be derived that

$$\left|\mathbf{V}_i^{\mathrm{H}}\mathbf{V}_j\right| = \left|\mathbf{Z}_m^{\mathrm{H}}\mathbf{F}_i^{\mathrm{H}}\left(\mathbf{F}(f_{mi})^{\mathrm{H}}\mathbf{F}(f_{mj})\right)\mathbf{F}_j\mathbf{Z}_m\right| \ll \mathbf{V}_i^{\mathrm{H}}\mathbf{V}_i, i \neq j. \tag{30}$$

(3). To some approximation, extracting interference does not take away any information of the NQR signal or any other frequency components of $\mathbf{Z}_m$. As the energy of $\mathbf{Z}_m^{(l)}$ can be written as $E^{(l)}=\left(\mathbf{Z}_m^{(l)}\right)^{\mathrm{H}}\mathbf{Z}_m^{(l)}$, we have

$$\begin{aligned} E^{(l)} &= \left(\mathbf{Z}_m - \mathbb{G}\mathbb{G}^{\dagger}\mathbf{Z}_m\right)^{\mathrm{H}}\left(\mathbf{Z}_m - \mathbb{G}\mathbb{G}^{\dagger}\mathbf{Z}_m\right) \\ &= \mathbf{Z}_m^{\mathrm{H}}\mathbf{Z}_m - \mathbf{Z}_m^{\mathrm{H}}\mathbb{G}\mathbb{G}^{\dagger}\mathbf{Z}_m = \mathbf{Z}_m^{\mathrm{H}}\mathbf{Z}_m - \mathbf{Z}_m^{\mathrm{H}}\mathbb{G}\mathbb{G}^{\dagger}\mathbb{G}\mathbb{G}^{\dagger}\mathbf{Z}_m \\ &= \mathbf{Z}_m^{\mathrm{H}}\mathbf{Z}_m - \left(\mathbb{G}\mathbb{G}^{\dagger}\mathbf{Z}_m\right)^{\mathrm{H}}\mathbb{G}\mathbb{G}^{\dagger}\mathbf{Z}_m, \end{aligned} \tag{31}$$

where $\mathbf{Z}_m^{\mathrm{H}}\mathbf{Z}_m$ and $\left(\mathbb{G}\mathbb{G}^{\dagger}\mathbf{Z}_m\right)^{\mathrm{H}}\mathbb{G}\mathbb{G}^{\dagger}\mathbf{Z}_m$ are the enegry of the data $\mathbf{Z}_m$ and the extracted components from $\mathbf{Z}_m$, respectively. In fact, based on Eqs. (29) and (30), we have

$$\begin{aligned} \left(\mathbb{G}\mathbb{G}^{\dagger}\mathbf{Z}_m\right)^{\mathrm{H}}\mathbb{G}\mathbb{G}^{\dagger}\mathbf{Z}_m &= \left(\sum_{i=1}^{l}\mathbf{F}(f_{mi})\mathbf{F}_i\mathbf{Z}_m\right)^{\mathrm{H}}\left(\sum_{i=1}^{l}\mathbf{F}(f_{mi})\mathbf{F}_i\mathbf{Z}_m\right) \\ &\simeq \sum_{i=1}^{l}\mathbf{Z}_m^{\mathrm{H}}\mathbf{F}_i^{\mathrm{H}}\mathbf{F}(f_{mi})^{\mathrm{H}}\mathbf{F}(f_{mi})\mathbf{F}_i\mathbf{Z}_m \\ &= \sum_{i=1}^{l}\mathbf{V}_i^{\mathrm{H}}\mathbf{V}_i, \end{aligned} \tag{32}$$

which means that we can approximately consider that the energy of each extracted frequency component does not contain the energy of any other frequency component in $\mathbf{Z}_m$. To summarize, as the main frequencies of the interference are known approximately, using Eq. (22) to cancel interference will not distort the information of the NQR signal.

ACKNOWLEDGMENTS

This work has been supported by Find a Better Way (FABW) UK, under Project AQUAREOS. The authors would like to thank Professor Andreas Jakobsson from Lund University, whose valuable input has improved the quality of the manuscript.

REFERENCES

[1] J. A. S. Smith, "Nuclear quadrupole resonance spectroscopy", J. Chem. Educ., **48**(1), 39-48(1971).

[2] N. R. Butt, E. Gudmundson, and A. Jakobsson, "An Overview of NQR Signal Detection Algorithms", *Magnetic Resonance Detection of Explosives and Illicit Materials*, Springer Netherlands, 2014; Part I, pp 19-33.

[3] J. Barras, D. Murnane, K. Althoefer, S. Assi, M. D. Rowe, I. Poplett, G. Kyriakidou, and J. A. S. Smith, "Nitrogen-14 Nuclear quadrupole resonance Spectroscopy: a promising new analytical methodology for medicines authentication and counterfeit antimalarial analysis", Analytical Chemistry, **84**, 2746-2753(2013).

[4] J. Barras, K. Althoefer, M. D. Rowe, I. J. P. Poplett, and J. A. S. Smith, "The Emerging Field of Nuclear Qudrupole Resonance-Based Medicines Authentication", Appl. Magn. Reson. **43**, 511-529(2012).

[5] A. Jakobsson, M. Mossberg, M. D. Rowe, and J. A. S. Smith, "Exploiting temperature dependency in the detection of NQR signals", IEEE Transactions on Signal Processing, **54**(5), 1610-1616(2006).

[6] A. Jakobsson, M. Mossberg, M. D. Rowe, and J. A. S. Smith, "Frequency-selective detection of nuclear quadrupole resonance signals", IEEE Trans. Geosc. Remote Sensing, **43**(11), 2659-2665(2005).

[7] M. D. Rowe, and J. A. S. Smith, "Mine Detection by Nuclear Quadrupole Resonance", in Proc. EUREL Int. Conf. on the Detection of Abandoned Land Mines, Oct. 1996, pp.62-66.

[8] A. Gregorovič, and T. Apih, "Relaxation during spin-lock spin-echo pulse sequence in N 14 nuclear quadrupole resonance", J. Chem. Phys., **129**, 214504(2008).

[9] S. D. Somasundaram, A. Jakobsson, J. A. S. Smith, and K. Althoefer, "Exploiting spin echo decay in the detection of nuclear quadrupole resonance signals", IEEE Trans. Geosc. Remote Sensing, **45**, 925-933(2007).

[10] J. Swärd, and A. Jakobsson, "Canceling Stationary Interference Signals Exploiting Secondary Data", European Signal Processing Conference, 2014, pp.1014-1018.

[11] G. Liu, Y. Jiang, H. Xiong, J. Li, and G. Barrall, "Radio frequency interference suppression for landmine detection by quadrupole resonance", EURASIP J. Applied SP, **2006**, 29890(2006).

[12] N. R. Butt, A. Jakobsson, S. D. Somasundaram, and J. A. S. Smith, "Robust Multichannel Detection of Mixtures Using Nuclear Quadrupole Resonance", IEEE Trans. Signal Process., **56**(10), 5042-

5050(2008).

[13] Y. Jiang, P. Stoica, and J. Li, "Array Signal Processing in the Known Waveform and Steering Vector Case", IEEE Trans. Signal Process., **52**(1), 23-35(2004).

[14] P. Stoica, H. Xiong, L. Xu, and J. Li, "Adaptive beamforming for quadrupole resonance", Digit. Signal Process., **17**, 634-651(2007).

[15] S. D. Somasundaram, "Advanced signal processing algorithms based on novel nuclear quadrupole resonance models for the detection of explosives", PhD thesis, King's College London, 2007.

[16] S. M. Kay, Fundamentals of Statistical Signal Processing, Volume II: Detection Theory. Englewood Cliffs, NJ: Prentice-Hall, 1998.

[17] M. R. Hestenes, and E. Stiefel, "Methods of conjugate gradients for solving linear systems", Journal of Research of the National Bureau of Standards, **49**, 409-436(1952).